

COSMIC ALIGNMENT TOWARDS THE RADIO EINSTEIN RING PKS 1830–211¹ ?

F. COURBIN²

Institut d’Astrophysique et de Géophysique, Université de Liège, Allée du 6 Août 17,
Sart Tilman (Bat. B5C), Liège 1, Belgium, Frederic.Courbin@ulg.ac.be

G. MEYLAN³

Space Telescope Science Institute, 3700 San Martin Drive, Baltimore, MD 21218, U.S.A., gmeylan@stsci.edu

J.-P. KNEIB

Observatoire Midi-Pyrénées, Laboratoire d’Astrophysique, UMR5572, 14 Avenue Edouard Belin,
31000 Toulouse, France, kneib@ast.obs-mip.fr

C. LIDMAN

European Southern Observatory, Casilla 19001, Santiago 19, Chile, clidman@eso.org
Draft version November 6, 2018

ABSTRACT

Optical and near-IR Hubble Space Telescope and Gemini-North adaptive optics images, further improved through deconvolution, are used to explore the gravitationally lensed radio source PKS 1830–211. The line of sight to the quasar at $z = 2.507$ appears to be very busy, with the presence, within $0.5''$ from the source of: (i) a possible galactic main-sequence star, (ii) a faint red lensing galaxy visible only in H -band and (iii) a new object whose colors and morphology match those of an almost face-on spiral. The $V - I$ color and faint I magnitude of the latter suggest that it is associated with the molecular absorber seen towards PKS 1830–211, at $z = 0.89$ rather than with the $z = 0.19$ HI absorber previously reported in the spectrum of PKS 1830–211. While this discovery might ease the interpretation of the observed absorption lines, it also complicates the modeling of the lensing potential well, hence decreasing the interest in using this system as a mean to measure H_0 through the time delay between the lensed images. This is the first case of a quasar lensed by an almost face-on spiral galaxy.

Subject headings: cosmology: observations — gravitational lensing — quasars: individual
(PKS 1830–211)

1. HISTORICAL CONTEXT

This paper presents a new step in the long series of studies trying to unveil the properties of the gravitationally lensed quasar PKS 1830–211. The object has a heavily populated line of sight, crowded by galactic and extragalactic objects. We start this introduction with a few highlights of what has been a particularly slow discovery process.

The radio source PKS 1830–211 was first detected as a single source in the Parkes survey (Shimmins et al. 1969) and soon recognized as one of the brightest sources at centimeter wavelengths. About twenty years later, high spatial resolution VLA observations at 1.5, 5, and 15 GHz unveiled the double structure of this otherwise flat-spectrum source (Rao et al. 1988). These authors immediately mentioned gravitational lensing as the best qualitative explanation for the presence of the two components, their separation, their flux ratios, and their almost identical substructures with a point inversion symmetry with respect to each other. Further high-resolution VLA observations at 5, 15 and 22.5 GHz provided enough information to allow theoretical modeling of the lensing effect, in spite

of the unknown redshifts of both the source and the lens (Subrahmanyan et al. 1990).

Deeper VLBI, Merlin and VLA observations, at 2.3, 1.7 and 8.4 GHz, respectively, showed an unusual elliptical ring-like structure connecting the two brighter components (Jauncey et al. 1991). This further favored the gravitational lens explanation, specifically, an Einstein ring formed by the gravitational imaging of a background radio source by a foreground mass concentration. Extensive theoretical modeling studies which reproduced successfully the ring and the two bright components were soon published (Kochanek & Narayan 1992, Nair et al. 1993).

Since the line of sight to PKS 1830–211 passes the galactic bulge (galactic longitude $l = 12.2$ deg and galactic latitude $b = -5.7$ deg), earlier attempts to identify the source and the lens failed because of source confusion, faintness, and poor spatial resolution. No visible counterpart was found down to $B \simeq 23$ mag. A relatively bright object, nearly coincident with the North-East component of the radio source, was identified spectroscopically with the Palomar 200-inch telescope as a foreground M star (Djorgovski et al. 1992). Extensive theoretical modeling studies

¹ Based on observations made with the NASA/ESA Hubble Space Telescope, obtained from the Data Archive at the Space Telescope Science Institute, which is operated by the Association of Universities for Research in Astronomy, Inc., under NASA contract NAS 5-26555. The HST data used here come from the archives related to the programs # 7495, # 8804, and # 9133 (CASTLES). This study is also based on observations made with the NOAO Gemini-North Telescope; NOAO is operated by the Association of Universities for Research in Astronomy (AURA), Inc. under cooperative agreement with the National Science Foundation.

² Pontificia Universidad Católica de Chile, Departamento de Astronomía y Astrofísica, Casilla 306, Santiago 22, Chile.

³ Affiliated with the Astrophysics Division of the European Space Agency, ESTEC, Noordwijk, The Netherlands.

which reproduced successfully the ring and the two bright components were soon published (Kochanek & Narayan 1992, Nair et al. 1993).

Wiklind & Combes (1996) identified 12 molecular absorption lines in a millimeter spectrum of PKS 1830–211 taken with the 15-m SEST/ESO telescope. They inferred that the lines originate in the lensing galaxy at $z=0.89$ and that the lens is a spiral, since the molecular abundances are compatible with Milky Way values. Lovell et al. (1996) observed HI absorption at $z = 0.19$ in Parkes data, indicating the presence of another galaxy at this redshift and pointing towards a possible compound lens (see also Frye et al. 1997). The $z=0.89$ redshift value was confirmed by Mathur & Nair (1997) who observed strong absorption features in their X-ray spectrum acquired with the Rosat/PSPC. HI absorption is also seen at $z=0.89$ (Chengalur et al. 1999). Further observations made at the 30-m IRAM and 15-m SEST/ESO telescopes confirmed the presence of two absorption lines at $z = 0.89$, one corresponding to the South-West lensed image of the background source, and the other, shifted in velocity by -147 km s^{-1} , corresponding to the North-East image. This implied that the background radio source is situated at a redshift of about 3 and consistent with the lensing galaxy being an early-type spiral seen almost face-on (Wiklind & Combes 1998; see also Swift et al. 2001).

At that stage, models predicted time delays of the order of one day to several tens of days for reasonable range of source and lens redshifts (Nair et al. 1992). This expectation and the fact that PKS 1830–211 varies regularly on time-scales of months made this object an ideal target, at that time, for determining a time delay between the lensed components. VLA observations at 8.4 and 15 GHz over a period of 13 months provided a first estimate $\Delta t = 44 \pm 9$ days (Ommen et al. 1995). More recently, ATCA observations at 8.6 GHz over a period of 18 months provided a second — inconsistent — estimate $\Delta t = 26 \pm 5$ days (Lovell et al. 1998). Since the redshift of the source was unknown and the lensing galaxy poorly parameterized, no estimate of H_0 was obtained. Microlensing, as deduced from ASCA X-ray observations (Oshima et al. 2001), may complicate the computation of the time delay.

It was only with the advent of a powerful deconvolution method (Magain et al. 1998) that significant progress was made in identifying the optical-infrared counterparts of PKS 1830–211. Near-infrared J and K images obtained at the 2.2-m MPI/ESO telescope and I and K images with the Keck I telescope, all with sub-arcsecond seeing, were deconvolved by Courbin et al. (1998). Both counterparts of the flat-spectrum core of the radio source were searched for. The M star identified by Djorgovski et al. (1992) was clearly separated from the bright North-East component of the quasar, whose radio and optical positions were shown to be identical. The South-West radio component, with similar radio flux, was not unambiguously identified with the optical object, because of mismatches between the positions of the source in the I , J , and K bands, and with its radio position as well. This object, much fainter in I , J and K than in the radio, was possibly identified with the lensing galaxy alone or a blend of various objects. The source counterparts are very red with $I - K \sim 7$, which suggests strong absorption from the Galaxy, the lensing

galaxy or both.

The brightness of the source at near-infrared wavelengths enabled the redshift of the source ($z=2.507 \pm 0.002$) to be determined with infra-red spectroscopy (Lidman et al. 1999).

Using intrinsically high spatial resolution images obtained with the Hubble Space Telescope in the near infrared (I with WFPC2/HST and H, K with NIC2/HST), Lehár et al. (2000) confirmed and improved the earlier quasar component identifications proposed by Courbin et al. (1998) with their ground-based deconvolved data. In addition, Lehár et al. (2000) identified an object that they associated with the lensing galaxy (lens G in Lehár et al. 2000 and in the following).

In this paper we present new results obtained from the deconvolution of deep imaging archive data obtained with the Hubble Space Telescope at visible and near-IR wavelengths, namely, WFPC2/F555W/F814W and NICMOS2/F160W/F205W. In addition, we use some new ground-based K -band adaptive optics images from the Gemini-North/Hokupa'a Adaptive Optics (AO) system, further improved with deconvolution. These observations in four broad-band filters, viz., V, I, H , and K , allow us to detect very clearly the arms of a spiral galaxy between the two quasar images. In addition to this new object, two other objects are seen along the line of sight: (i) a red point source that might be either the bulge of the spiral or a galactic star, and (ii) a very faint and red object seen only in H , at the position of the object G previously reported by Lehár et al. (2000).

2. OBSERVATIONS

2.1. Hubble Space Telescope Imaging

The Hubble Space Telescope observations presented in this paper are public and available in the archives. They were obtained as part of GO programs (PI: E. Falco with ID # 7495, # 8804, and # 9133) known as the CfA-Arizona Space Telescope LENS Survey (CASTLES), and aimed at imaging with the HST all known gravitationally lensed quasars. The near-IR data, viz., WFPC2/F555W/F814W and NIC2/F160W/205W, collected by CASTLES for PKS 1830–211 were used in their study of 10 two-image gravitational lenses (Lehár et al. 2000), where the observing details can be found.

We re-analyse here these data, using deconvolution techniques for further improvement. We take also advantage of the fact that, since the publication of Lehár et al. (2000), much deeper WFPC2/F814W images were obtained (program ID # 8804), corresponding to four times 1,200 sec, in addition to the four 400-sec exposures already published. These additional data allow us to discover an almost face-on spiral galaxy acting as a gravitational lens on PKS 1830–211 (see below). We also detect this galaxy in new WFPC2/F555W data (3 images, for a total of 2,000 sec; program ID # 9133), however very close to the detection limit.

2.2. Gemini/Hokupa'a Adaptive Optics Imaging

The above HST data are supplemented by ground-based K -band adaptive optics (AO) images of PKS 1830–211, obtained during the night of 2000 August 8th, with the Hokupa'a instrument mounted on the 8.2-m Gemini-North

telescope at Mauna Kea, Hawaii. The raw data have excellent sampling ($0.020''$ per pixel) and fairly good image quality ($\text{FWHM} = 0.15''$). The reduced data before deconvolution is presented in Figure 1, where the two quasar images are seen, well separated, as well as the $V \sim 13.5$ mag star used for the wavefront correction, about $7''$ to the North-East of PKS 1830–211. Due to the high airmass of the object (between 1.5 and 2.2) and to the relatively faint guide star, the wavefront correction was not fully satisfactory, with a final seeing about twice as large as the diffraction limit of an 8.2-m telescope in the K -band. These images are rather shallow, with a total exposure time of 30 minutes, but they nevertheless allow the measurement of the positions of the quasar images with an accuracy better than could be done with the HST data alone. No standard star was observed, as the observations were performed through thin cirrus.

These data are the first images of a gravitational lens taken with AO on a 10-m class telescope. The presence of a suitable wavefront guide star and many PSF stars should allow one to improve the present result if the observations can be repeated at a smaller airmass and with much longer exposure time. Given the low declination of PKS 1830-211, the Paranal Observatory is ideally located for such observations.

3. ASTROMETRY — PHOTOMETRY

All the data are deconvolved with the MCS deconvolution algorithm which results in images with improved resolution and sampling (see Courbin et al. 1998 for more details about the application of this method). The spatial resolution of the final images is $0.046''$ for the WFPC2/F555W/F814W data, $0.075''$ for the HST NIC2/F160W/F205W near-IR data, and $0.020''$ for the Gemini K -band data.

Figures 2, 3, and 4 show the resulting deconvolved images. In all cases but for the F205W filter, the result of the deconvolution process is good, as several PSF stars are available in the immediate vicinity of the deconvolved field.

Since the objects in the vicinity of PKS 1830-211 have very different colours, astrometry is performed in all available bands, taking as a reference coordinate system the best and deepest data available, i.e., the HST F814W image. The transformation between the astrometry of the different bands into the coordinate system of the F814W image is done by using stars seen simultaneously in all filters. Tables 1 and 2 gives the photometric and astrometric results for all selected objects (see Section 4 for the meaning of the object labeling that we keep as in Lehár et al. 2000).

The photometry and astrometry are always performed on the deconvolved images in order to avoid mutual contamination of the extended and unresolved objects. We used the same zero points as in Lehár et al. (2000). The magnitude of extended objects are measured in apertures of $0.5''$ in diameter. As PKS 1830-211 is situated at low galactic latitude, we have corrected the photometry for galactic absorption. From the DIRBE/IRAS maps of Schlegel et al. (1998), Kochanek et al. (2002) estimate $E(B-V)=0.464$ towards the PKS 1830-211. We correct our photometry using this value and a mean galactic absorp-

tion law with $R_V=3.1$ (Savage & Mathis, 1979). The results are indicated in Table 1. Note that while the correction is reasonable for extragalactic objects, it might be an over-estimate for galactic objects such as object S1 and P.

4. STARS AND GALAXIES TOWARDS PKS 1830–211 ?

With these observations of improved spatial resolution, greater spectral coverage and greater depth, it is easier (but still challenging) to identify the different objects along the line of sight to PKS 1830–211.

4.1. Stars

The two quasar images are seen simultaneously with a decent signal-to-noise only in the K -band, i.e., on the HST F205W images and on the Gemini data. The M-star, observed spectroscopically by Djorgovski et al. (1992) and labeled S1 in Lehár et al. (2000), is seen at all wavelengths. The total field contains also numerous galactic stars, given the low galactic latitude of the quasar, viz., $b = -5.7$ deg.

One point-like object is seen between the two quasar images. It is labeled P in Lehár et al. (2000) and in Figures 2-7, and remains unresolved even in the deep deconvolved F814W image, in spite of the high signal-to-noise. The shallow depth of the Gemini images and the complicated PSF in the HST images do not allow us to constrain the shape of object P. We construct the color-magnitude diagram for 89 objects in the field immediately surrounding PKS 1830–211 (Fig. 7), and find that object P falls in the bulk of faint main-sequence stars. This diagram has to be taken with caution since the stars are spread over a broad range of distances, metallicities and reddening values. Still, it is indicative that object P might be a galactic star seen on the line of sight to PKS 1830–211.

Star S1 was identified as an M dwarf by Djorgovski et al. (1992) from a Palomar 200-inch spectrum. From our photometry in Table 1 (we use here the magnitude not corrected for galactic reddening), we have $m_V(S1) = 22.18$ and $m_V(P) = 26.20$ with $(V - K)_{S1} = 5.46$ and $(V - K)_P = 5.13$. Such colors point towards M dwarf stars, in agreement with Djorgovski et al. (1992). A value $V - K \sim 5.3$ corresponds to an M4 dwarf, which has a absolute magnitude $M_V \sim 11$. If both S1 and P objects were M4 dwarfs, they would be located, ignoring any reddening, at a distance 1.7 and 11.0 kpc, respectively. If we adopt 10 km s^{-1} as a typical lower limit for the transverse velocity, these objects would have proper motions of 1 mas yr^{-1} and 0.2 mas yr^{-1} , respectively. In WFPC2 frames, positions of stars have been measured with an accuracy of about 0.02 pixel (Anderson & King 2000), which corresponds to 1 mas on the PC of HST. in the PC frames. The HST observations in the F814W filter are split into two epochs separated by 529 days. After carefully comparing these frames, neither S1 nor P show significant proper motions. However, a time baseline of a few more years may allow the detection of some proper motions, which would confirm the stellar character of these two objects.

4.2. Galaxies

Two more objects are visible between the two quasar images. One, labeled G in Lehár et al. (2000), is seen without ambiguity only in the F160W image. It is completely invisible in the F555W and F814W images, and

it is heavily contaminated by the PSF of nearby point sources in the F205W image. We are able to measure its F160W magnitude, but disagree with the result of Lehár et al. (2000) by more than one magnitude. Since there is no such discrepancy for all the other objects in the field, a plausible explanation is contamination by PSF residuals, acting in different ways in our deconvolved images and the PSF subtracted images of Lehár et al. (2000). Note that there are PSF residuals visible on the deconvolved F160W image. These are due to differences between the PSF used for the deconvolution and the actual one of the data. They are prominent near the bright point sources S1 and QSO A. For fainter sources such as star P or QSO B, they become negligible, as they are scaled down well below the noise level. Note that they are not visible close to the faint stars to the West of the field, hence even less near the fainter sources such as star P and QSO B. Object G can therefore be considered as real. It was identified by Lehár et al. (2000) as the one responsible for the molecular absorption lines observed at $z = 0.89$ in the quasar spectra.

The F555W and F814W images allow the detection of a second new object, to the South of object P. Only the brightest parts of this object are visible in the shallow F814W data of Lehár et al. (2000). However, with the new, much deeper exposures, two conspicuous spiral arms appear on both sides of a brighter spot (Lens SP in Tables 1-2 and in Figures 2-6), which we identify as a possible position for the bulge of an almost face-on spiral. The putative bulge of the spiral is indicated by a circle in the Figures 2-4 and labeled “lens SP”. Note that given the lack of resolution of the data, even after deconvolution, the bulge of galaxy SP is not well defined. Therefore, we consider its center as the barycenter of the area defined by the spiral arms. It is labeled Center SA in Table 2 and in Figure 2. Given the uncertainties, it is one of the three possible centers considered in our modeling. Using the F205W HST data and the Gemini data, we find that the extremely red image B of the quasar is exactly superposed with one of the spiral arms, which explains its faintness in the optical. This is clearly visible in Figure 2 but it can also be seen in the “true-color” images shown in Figures 5 and 6, which help to mentally visualize the redshift information of the data. The first image (Fig. 5) is a composite of 3 images, through the F814W, F160W, and F205W filters. It shows the two reddened quasar images and the central star P, which has the same color as the field stars. Due to contamination by the bright quasar images, it is difficult in this image to see clearly the two lensing galaxies. Fig. 6 does not use the F205W frame, where the quasars are very bright. This image is composed of the F814W image as the blue channel, the F160W as the red channel and the mean of the F814W and F160W as the green channel. The objects between the quasar images are now easily seen, with the face-on spiral lens in blue (note the blue arm passing in front of quasar image B) and the much redder lens G, in green.

The spiral lens SP is very faint, but detected, in the F555W image. We infer a $V - I$ color of 0.8 ± 0.5 which is not well enough constrained to set a first redshift estimate. However, the very faint V and I -band magnitudes themselves indicate a relatively high redshift, given the mor-

phological type of the object. This, in combination with the fact that the spiral arms are seen right in front of the heavily reddened South-West quasar component, makes it very likely that we have discovered the spiral responsible for the CO, HCO+, HCN and HNC absorptions at $z = 0.89$. We stress, however, that we can not completely exclude a much lower redshift, for example $z = 0.19$, given the photometric error bars.

5. MODELING

In spite of the complexity of the system, one can attempt to model the different components of the lens using the few available constraints (position and flux ratio) and try to infer what might the correct lens configuration be. We have considered here Pseudo-Isothermal-Elliptical-Mass-Distributions (PIEMD), as used for example in Burud et al. (2002) and Kneib et al. (1996). Note however that the results quoted here depend only weakly on the exact mass profile chosen. We have considered the flux ratio between the quasar components to be the one observed in the radio, unaffected by dust, i.e., $F_A/F_B = 1$. We chose a “realistic” cosmology with $H_0 = 65 \text{ km s}^{-1} \text{ Mpc}^{-1}$, $\Lambda = 0.7$, and $\Omega_M = 0.3$.

First, we consider a single mass distribution centered at different plausible locations: galaxy G, galaxy SP and the barycenter of the spiral arms SA. Only for position G and SA, could we obtain a good fit using an elliptical mass model with a predicted time-delay of about 40 days at position G and 31 days at position SA. Changing the observed flux ratio to $F_A/F_B = 1.5$ as measured by Lovell et al. (1998) does not significantly change the predicted time-delay. Centering the mass distribution on star P, assuming it is the bulge of the lensing galaxy, predicts time-delays that are much higher than what is observed, for reasonable values of H_0 .

Next, we consider two lens models with the lenses centered on G and SP. For simplicity, we assume G and SP to be at the same redshift, i.e., $z=0.89$, with only the velocity dispersion of the two galaxies as a free parameter. For circular mass distributions a good fit could not be found (reduced $\chi^2 = 25$), and the mass of G was found to be 3 times larger than SP. We therefore added ellipticity. We found that if $\epsilon \sim 0.2$ and $\text{PA} = -50^\circ$ a good fit is achieved with a mass ratio (G over SP) of 3.5. However, the models never predict a time delay much lower than 40 days, highly incompatible with the observe one ($\Delta t = 26 \pm 5$ days). This was already pointed out in Lehár et al. (2000), who find unrealistically high values for the Hubble parameter if the whole lensing potential were to be due to lens G alone. Changing the observed flux ratio to $F_A/F_B = 1.5$ does not improve the situation.

Decreasing the redshifts of the two lenses G and SP to $z=0.19$ can also be used to fit the data (with an elliptical mass distribution for G), but of course predict very low time delays, of the order of 10 days. We have therefore considered a model composed of only galaxy G (the most massive of the two) and of the large spiral galaxy seen a few arcsec to the SW of PKS 1830-211, which will introduce some external shear. As in the model with two lenses (G+SP), no decent fit can be obtained if G is circular. Good fits are found by introducing an ellipticity, with $\epsilon > 0.3$, $\text{PA} \sim -90^\circ$. In this case, the predicted time-delay

($\Delta t \sim 32 \pm 4$ days - depending on the exact mass contribution of the lower redshift component) matches the observations. However, we reproduce the same range of time-delay with a model that consider only the lens G ($z=0.89$), but located $0.08''$ to the North of its observed position. Such a shift is large but not out of question given the astrometric error bars.

Constructing a model that matches all the constraints (position, flux ratio, time delay) is possible, especially when including the low redshift spiral galaxy to the SW of the quasar. However, in order to use PKS 1830-211 to constrain H_0 , much better observational information is required in order to characterise the various mass component along the line of sight to PKS 1830-211 and to ascertain the exact nature and reality of all intervening objects.

6. CONCLUSION

The lensing potential in PKS 1830-211 is composed of one face-on spiral galaxy with a poorly defined center and probably at $z=0.89$, galaxy G also with a poorly defined center and unknown redshift and a third galaxy, possibly at $z=0.19$. With two and probably three galaxies contributing to the lensing effect, we conclude that it will be difficult to successfully model the system with an accuracy comparable to that reached for other simpler systems.

Unless more observational constraints become available, in particular the precise redshifts and positions of the lenses, PKS 1830–211 will remain of little interest in terms of modeling and for the determination of H_0 , even though the time delay is now measured with good accuracy. Nevertheless, PKS1830-211 is important for the study of absorption lines, microlensing and absorption by

dust.

PKS 1830-211 illustrates very well the need for high spatial resolution in quasar lensing studies. Modeling of this complicated system will not only require the redshift measurement of the lenses, but also the discovery of more lensed sources so that the lensing potential can be probed in more than just the two points given by the quasar images. The host galaxy of the quasar can be used to further improve the models, and arcs or arclets might appear at very high spatial resolution. Such data will only become available with the next generation of space instruments or with AO systems mounted on large telescopes, possibly coupled with integral field spectrographs.

Note: After the submission of this paper, Winn et al. (2002) analysed some of the present data independently, and concluded that star P is the bulge of one single lensing galaxy. This hypothesis is also plausible and modeling of the system is given by Winn et al. (2002).

The multi-band HST archives data used in this paper were obtained by the CfA-Arizona Space Telescope LENS Survey (CASTLES). We warmly thank Roser Pello for her help with the redshift estimates, and Tommy Wiklind for useful discussions. Frédéric Courbin is supported by Chilean grant FONDECYT 3990024, by the European Southern Observatory, and by Marie Curie grant MCFI-2001-0242. Two collaborative grants between Chile and France are also gratefully acknowledged: ECOS/CONICYT CU00U05 and CNRS/CONICYT 8730. Jean-Paul Kneib acknowledges support from French CNRS.

REFERENCES

- Anderson, J., King, I.R., 2000, PASP, 112, 1360
 Burud, I., Courbin, F., Magain, P., et al. 2002, A&A 383, 71
 Chengalur, J.N., de Bruyn, A. G., Narasimha, D., 1999, A&A 343, L79
 Courbin, F., Lidman, C., Frye, B.L., et al., 1998, ApJ, 499, L119
 Djorgovski, S.G., Meylan, G., Klemola, A., et al. 1992, MNRAS, 257, 240
 Frye, B.L., Welch, W.J., & Broadhurst, T.J., 1997, ApJ, 478, L25
 Jauncey, D.L., Reynolds, J.E., Tzioumis, A.K., et al. 1991, Nature, 352, 132
 Kennicutt, R.C., 1992, ApJS, 79, 255
 Kneib J.-P., Ellis R. S., Smail I., et al. 1996, ApJ 471, 643
 Kochanek, C.S., Falco, E.E., Impey, C., et al., 2002, <http://cfa-www.harvard.edu/glensdata/>
 Kochanek, C.S., Falco, E.E., Impey, C.D., et al., 2000, ApJ, 401, 461
 Kochanek, C.S., & Narayan, R., 1992, ApJ, 401, 461
 Lehár, J., Falco, E.E., Kochanek, C.S., et al., 2000, ApJ, 536, 584
 Lidman, C., Courbin, F., Meylan, G., et al., 1999, ApJ, 514, L57
 Lovell, J.E.J., Reynolds, J.E., Jauncey, D.L., et al., 1996, ApJ, 472, L5
 Lovell, J.E.J., Jauncey, D.L., Reynolds, J.E., et al., 1998, ApJ, 508, L51
 Magain, P., Courbin, F., & Sohy, S., 1998, ApJ, 494, 472
 Mathur, S., & Nair, S., 1997, ApJ, 484, 140
 Nair, S., Narasimha, D., & Rao, A.P., 1993, ApJ, 407, 46
 Oshima, T., Mitsuda, K., Ota, N., et al., 2001, ApJ, 551, 929
 Rao, A.P., & Subrahmanyan, R. 1988, MNRAS, 231, 229
 Savage, B. D., Mathis, J. S., 1979, ARA&A, 17, 73
 Schlegel, D.J., Finkbeiner, D.P., Davis, M., 1998, ApJ, 500, 525
 Shimmings, A.J., Manchester, R.N., & Harris, B.J., 1969, Austral. J. Phys. Astrophys, Suppl., 8, 3
 Subrahmanyan, R., Narasimha, D., Rao, A.P., & Swarup, G., 1990, MNRAS, 246, 263
 Swift, J.J., Welch, W.J., & Frye, B.L., 2001, ApJ, 549, L29
 van Ommen, T.D., Jones, D.L., Preston, R.A., & Jauncey, D.L., 1995, ApJ, 444, 561
 Wiklind, T., & Combes, F., 1996, Nature, 379, 139
 Wiklind, T., & Combes, F., 1998, ApJ, 500, 129
 Winn, J.N., Kochanek, C.S., McLeod, B.A., et al. 2002, ApJ, this issue

TABLE 1
HST PHOTOMETRY OF THE OBJECTS ALONG THE LINE OF SIGHT TO PKS 1830–211.

Object	F555W WFPC2	F814W WFPC2	F160W NIC2	F205W NIC2
QSO A	25.62 ± 0.10 [24.19]	22.10 ± 0.03 [21.42]	17.04 ± 0.03 [16.82]	15.47 ± 0.01 [15.34]
QSO B	>26.50 [>25.07]	> 25.70 [>25.02]	22.82 ± 0.20 [22.60]	19.53 ± 0.03 [19.40]
Star S1 (M-type)	22.18 ± 0.05 [20.75]	19.43 ± 0.02 [18.75]	17.20 ± 0.03 [16.98]	16.72 ± 0.03 [16.59]
Star P	26.20 ± 0.30 [24.77]	23.72 ± 0.10 [23.04]	21.72 ± 0.20 [21.50]	21.07 ± 0.20 [20.94]
Lens G	21.12 ± 0.50 [20.90]	...
Lens SP	26.64 ± 0.40 [25.21]	25.10 ± 0.20 [24.42]
Low redshift lens ($z=0.19$?)	23.71 ± 0.05 [22.28]	22.10 ± 0.02 [21.42]	20.25 ± 0.05 [20.03]	19.55 ± 0.05 [19.42]

Note. — The magnitudes given for Lens G, Lens SP and the low redshift galaxy to the SW of PKS 1830-211 are measured on the deconvolved images, through apertures of $0.5''$ in diameter. Only the bulge of Lens SP is considered, the spiral arms are invisible in the F555W image. Magnitudes between brackets are corrected for galactic extinction.

TABLE 2
ASTROMETRY OF THE OBJECTS ALONG THE LINE OF SIGHT TO PKS 1830–211.

Object	X ($''$)	Y ($''$)
QSO A	0.0000	0.0000
QSO B	$+0.654 \pm 0.002$	-0.725 ± 0.002
Star S1 (M-type)	-0.091 ± 0.002	$+0.525 \pm 0.002$
Star P	$+0.327 \pm 0.004$	-0.491 ± 0.004
Lens G	$+0.519 \pm 0.080$	-0.511 ± 0.080
Lens SP	$+0.285 \pm 0.040$	-0.722 ± 0.040
Center SA for spiral lens	$+0.300 \pm 0.050$	-0.610 ± 0.050
Low redshift lens ($z=0.19$?)	-0.245 ± 0.050	-2.490 ± 0.050

Note. — As the different objects have very different colors, the astrometry is obtained from the best available filter and then matched to the coordinate system of the F814W image. In particular, QSO B is measured in the F205W image and in the Gemini *K*-band image. Star P, star S1 and the lens SP are measured in the F814W data. Lens G is measured from the F160W data.

FIG. 1.— Gemini North + Hokupa’a K -band image of the field surrounding PKS 1830-211. The guide star used for the wavefront measurement is indicated. The image quality on this 30-minute exposure is $0.14''$. This is twice the diffraction limit, but is still twice as good as the HST in this band. The two quasar images and the M-type star S1 are already well separated on this un-deconvolved image.

FIG. 2.— **Left:** Part of the HST/WFPC2 image of PKS 1830-211. This image is a combination of all available frames in the F814W filter (8 in total), for a total exposure time of 6,400 sec. **Right:** Simultaneous deconvolution of the 8 frames (see text), reaching a resolution of $0.046''$, and sampled with a pixel of $0.023''$. The various positions of the two probable lenses and of the very obscured (and hence invisible here) QSO B are indicated with circles. Note the obvious spiral shape between the quasar images, with one spiral arm passing right onto the line of sight to QSO B. We identify this galaxy as the probable source of absorption at $z = 0.89$. The center of the ellipse shown in this figure defines the barycenter SA of the spiral (see main text). It is one of three centers, together with SP and G, considered in the modelling. There is no significant trace in this image of the much redder lens G, but we plot its position as measured from the near-IR F160W image, in overlay on the F814W image.

FIG. 3.— **Left:** Part of the HST/NICMOS2 image of PKS 1830-211 obtained in the F160W filter (4 individual frames). **Right:** Simultaneous deconvolution of the four F160W images, with a final resolution of $0.075''$. Note the object right to the West of star P. Lens G is visible in this frame only. There is no trace of the spiral galaxy SP, which is marked with a circle.

FIG. 4.— **Left:** Gemini + Hokupa’a K -band image of PKS 1830-211. This image shows a zoom in the same data as in Fig. 1. **Right:** The simultaneous deconvolution of 8 stacks of images allows a resolution of $0.020''$ to be reached, sampled on a grid of pixels of $0.010''$. The data, too shallow to reveal the lensing galaxies, is useful to measure the positions of the quasar images, with a very high precision. The point-like object P (not modelled as a point source in the Gemini data) is clearly visible.

FIG. 5.— Composite image obtained from the central parts of the HST I (F814W), H (F160W), and K (F205W) band data. The different objects identified in the single band images are identified. Note the strong similarity between the colors of star P and the other stars in the field. The two quasar images, extremely reddened, are prominent in the red channel of the image (i.e., the K -band image). Lens SP is visible as a blue fuzz between the quasar images, while lens G, best seen in F160W, is visible as a greenish object (F160W being the green channel of the composite image). Note the low-redshift (?) galaxy to the south of the lensed quasar.

FIG. 6.— Same field as in Figure 5 but constructed with the I -band (F814W) data as the blue channel, the H -band (F160W) as the red channel, and the mean of the I and H -band images as the green channel. Light contamination by the quasar images affects much less the lens galaxies, which are clearly visible, either in blue (spiral lens SP) or green (lens G). Note the blue spiral arm passing at the position of quasar image B. The objects marked “??” are probably structures in the PSF of the H -band image. They are cleanly removed in the deconvolution in Fig. 3

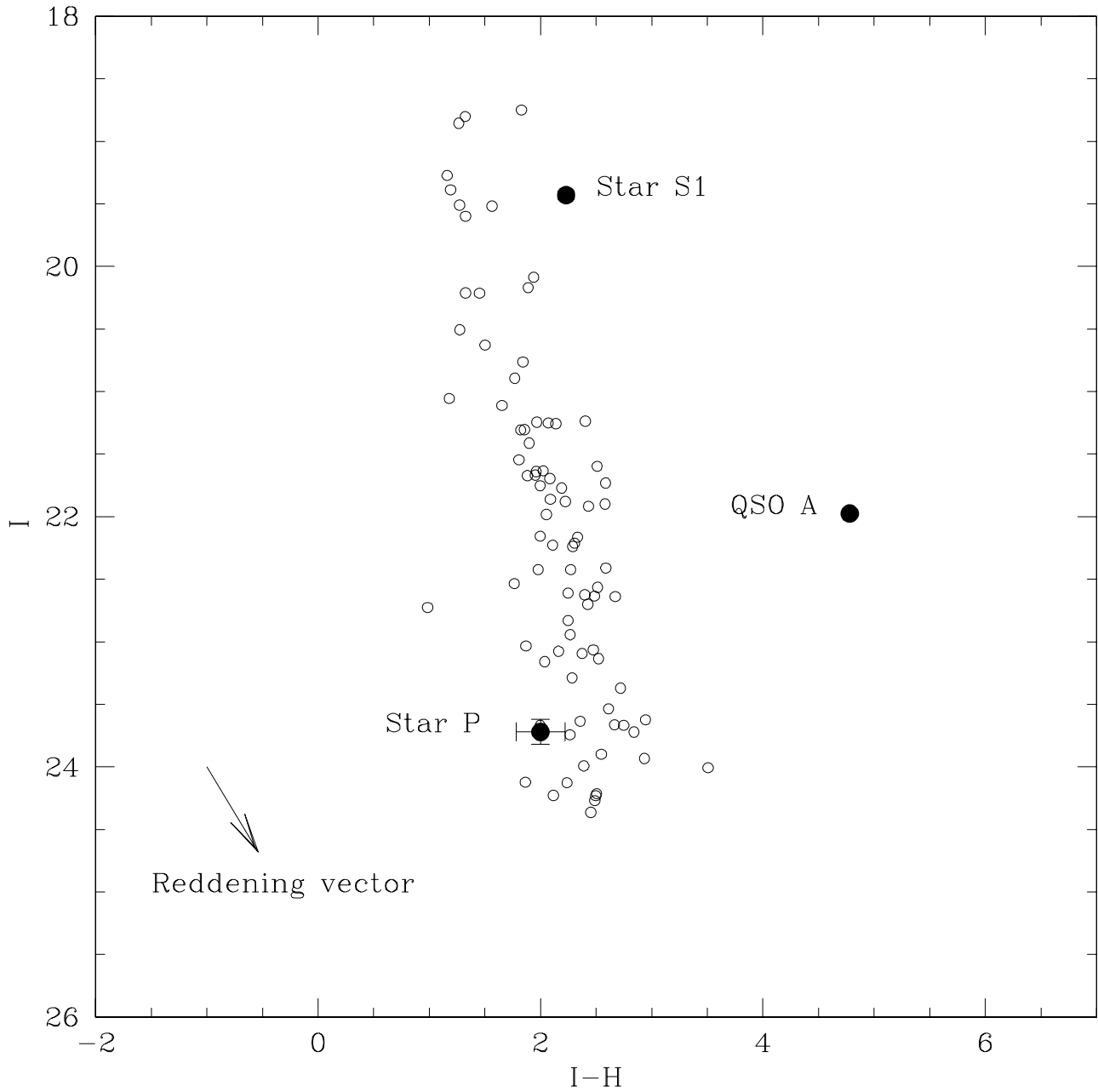


FIG. 7.— Color magnitude diagram for 89 objects around PKS 1830–211. The stellar main sequence is seen. When looking at this diagram, one should note that stars towards the Galactic bulge are spread over a broad range of distances, metallicities and reddenings. The open dots show the stars. The different objects of interest are plotted as larger black dots, such as QSO A, Star P and Star S1. Star P falls on the stellar main sequence, within the error bars. The data points are not de-reddened. The reddening vector is indicated.

This figure "fig01.gif" is available in "gif" format from:

<http://arxiv.org/ps/astro-ph/0202026v2>

This figure "fig02.gif" is available in "gif" format from:

<http://arxiv.org/ps/astro-ph/0202026v2>

This figure "fig03.gif" is available in "gif" format from:

<http://arxiv.org/ps/astro-ph/0202026v2>

This figure "fig04.gif" is available in "gif" format from:

<http://arxiv.org/ps/astro-ph/0202026v2>

This figure "fig05.gif" is available in "gif" format from:

<http://arxiv.org/ps/astro-ph/0202026v2>

This figure "fig06.gif" is available in "gif" format from:

<http://arxiv.org/ps/astro-ph/0202026v2>